



This is a repository copy of *A practical method for determining shear crack induced deformation in FRP RC beams*.

White Rose Research Online URL for this paper:  
<http://eprints.whiterose.ac.uk/104532/>

Version: Accepted Version

---

**Article:**

Imjai, T., Guadagnini, M. [orcid.org/0000-0003-2551-2187](https://orcid.org/0000-0003-2551-2187), Garcia, R. et al. (1 more author) (2016) A practical method for determining shear crack induced deformation in FRP RC beams. *Engineering Structures*, 126. pp. 353-364. ISSN 0141-0296

<https://doi.org/10.1016/j.engstruct.2016.08.007>

---

**Reuse**

This article is distributed under the terms of the Creative Commons Attribution-NonCommercial-NoDerivs (CC BY-NC-ND) licence. This licence only allows you to download this work and share it with others as long as you credit the authors, but you can't change the article in any way or use it commercially. More information and the full terms of the licence here: <https://creativecommons.org/licenses/>

**Takedown**

If you consider content in White Rose Research Online to be in breach of UK law, please notify us by emailing [eprints@whiterose.ac.uk](mailto:eprints@whiterose.ac.uk) including the URL of the record and the reason for the withdrawal request.



[eprints@whiterose.ac.uk](mailto:eprints@whiterose.ac.uk)  
<https://eprints.whiterose.ac.uk/>

# A practical method for determining shear crack induced deformation in FRP RC beams

Thanongsak Imjai<sup>\*a</sup>, Maurizio Guadagnini<sup>b</sup>, Reyes Garcia<sup>b</sup>, Kypros Pilakoutas<sup>b</sup>

<sup>a</sup> *Dept. of Civil Engineering, Rajamangala University of Technology Tawan-Ok, 225 Phayathai Road, Pathum-Wan, Bangkok, Thailand 10330*

<sup>b</sup> *Dept. of Civil and Structural Engineering, The University of Sheffield, Sir Frederick Mappin Building, Mappin Street, Sheffield, S1 3JD, UK.*

Tel.: +66 (0) 2 252 7029

Fax: +66 (0) 2 252 7580

Email (corresponding author\*): [thanongsak\\_im@rmutto.ac.th](mailto:thanongsak_im@rmutto.ac.th), [thanongsak.imjai@gmail.com](mailto:thanongsak.imjai@gmail.com)

## Abstract

This article proposes a practical semi-empirical method for determining shear crack-induced deformations in Glass Fibre Reinforced Polymer (GFRP) Reinforced Concrete (RC) beams. Current design guidelines neglect shear and shear crack-induced deformations in the calculation of deflections of GFRP RC beams. However, shear-induced deformations can be up to 30% of the total beam deflection due to the lower stiffness of GFRP bars compared to steel. To calculate the component of deflection due to shear action and crack opening, the proposed model uses a 'single fictitious inclined crack' with a width equal to the sum of the individual effective shear crack widths. Twelve shear tests were conducted on six RC beams reinforced internally with GFRP bars considering different reinforcement types and test parameters. The additional deformation due to shear cracks calculated by the proposed model is then used to predict the overall deformations of such beams up to failure. It is shown that, in comparison to current design guidelines, the proposed model predicts more accurately the total deflection of FRP RC beams at both service and ultimate loads. This article contributes towards the development of more accurate models to assess the overall shear deflection behaviour of FRP RC beams so as to balance the performance, serviceability and economic viability of structures.

**Keywords:** Shear cracks, Shear deformation, Deflection, FRP, Reinforced Concrete

# 1. Introduction

In the last two decades, the use of Fibre Reinforced Polymer (FRP) reinforcement has been widely adopted in the construction industry to address durability issues and to extend the service life of reinforced concrete (RC) beams. Nonetheless, due to the properties of FRP materials (high strength, relatively low elastic modulus, softer bond and elastic tensile response up to failure), FRP reinforced beams generally develop wider cracks compared to counterpart specimens reinforced with conventional steel reinforcement. As a result, such FRP RC beams also experience larger deflections that affect the aesthetics and structural performance of these elements. To ensure an acceptable level of structural performance, it is necessary to estimate accurately the maximum deflections (i.e. deformations) at serviceability limit state, as well as at higher load levels.

Overall, the sources of deformation in FRP RC beams subjected to flexure consist of the flexural, shear and rigid body components, as discussed later in Section 5 of this study. Shear induced deformations are normally negligible at service load and are usually ignored when calculating the total deflection of FRP RC members. However, previous research indicates that i) the component of shear induced deflection can be larger when FRP materials are used as reinforcement [1], and ii) shear deformations can increase rapidly after the development of diagonal cracks, thus reducing considerably the overall stiffness of the element [2, 3].

Moreover, experimental results on FRP RC beams [4, 5] also indicate that the development of diagonal cracking can result in additional deformations (up to 30% of the total deflection as shown later) that need to be taken into account. Despite of this, relatively few studies have examined in detail the shear behaviour of FRP RC beams (e.g. [1, 5-7]).

The overall deformation of RC beams depends heavily on cracking. The task of defining the magnitude of each individual deformation component (e.g. bending, shear and rigid body) as

well as any interaction between them is a challenging task. For instance, to date there is no standard method to measure accurately shear induced deformations, which in turn prevents compiling a comprehensive database of experimental results suitable for the development of improved predictive models. Due to this lack of robust data, current design recommendations calculate the deflections of FRP RC members using equations originally developed for steel reinforced concrete elements. However, such guidelines can underestimate overall deformations by up to 20% [4] as the shear deflection component is neglected in the calculations.

Whilst several studies have focused primarily on the development of models to estimate the shear strength of RC beams with FRP stirrups [e.g. 8-13], additional research has provided further insight into their deflection behaviour. For instance, several approaches available in the literature can predict accurately deflections of members subjected to flexure but only up to a service condition (e.g. [14-20]). Rafi and Nadjai [21] proposed modifications to the ACI 440 guidelines to improve the accuracy of the deflection predictions over the complete load history (e.g. from elastic to ultimate loads), although the proposed model did not consider the shear induced deformations. Kara et al. [20] proposed a stiffness matrix-based method to predict the deflection of FRP reinforced elements. Whilst the method calculates deflections with reasonable accuracy, it is computationally demanding and thus difficult to incorporate in design guidelines. Ferreira et al. [22] proposed a 1D fibre beam finite element (FE) model that accounts for the additional shear deformations in FRP RC beams. The FE model was proven effective at predicting the deflection of beams over the complete load history, but such FE analyses are mainly suitable for research purposes. More recently, Dundar et al. [23] presented a general computational algorithm to calculate deflections of FRP RC beams based on effective flexibilities of members in the cracked state using a) curvature distributions along the member, or b) available effective stiffness models. Using this model, Dundar et al.

predicted accurately the complete load-deflection history of FRP RC beams, but it is also necessary to verify the accuracy of such model using additional test data. Moreover, to date, practical models to predict the deflection of a FRP reinforced member throughout its complete load history are still needed.

This article proposes a practical method to determine shear crack induced deformations in FRP RC beams. Section 2 of this study discusses design equations included in recent design guidelines that predict deflections of FRP RC members. Subsequently, Section 3 presents an experimental programme on six beams designed to fail in shear. Section 4 presents and discusses the experimental observations, and gives details of the initiation and development of shear cracking, which are used as input parameter of the proposed method. The model is then incorporated into existing code equations to calculate the overall beam deformations up to failure (Section 5). The model is validated by comparing the predicted deflections and the experimental results from the tested beams. Concluding remarks of this study are given in Section 6. This article contributes towards the development of more accurate models to assess the overall shear deflection behaviour of FRP RC beams so as to balance the performance, serviceability and economic viability of structures.

## **2. Deflection prediction of FRP RC members**

Short-term deflections of FRP RC beams are generally derived using linear-elastic deflection equations that utilise an effective moment of inertia that accounts for stiffness losses due to cracking. Whilst many approaches are used to derive the effective moment of inertia of FRP RC beams [14-16], this study focusses on the widely adopted ACI 440 [24] and Eurocode 2 (EC2) [25] recommendations.

ACI 440 [24] adopts a modified form of Bischoff's [26] section-based equation for calculating the effective moment of inertia  $I_e$  (see Eq. 1), which includes a factor  $\gamma$  to account for the stiffness variation along the length of a flexural element:

$$I_e = \frac{I_{cr}}{1 - \gamma \left(\frac{M_{cr}}{M_a}\right)^2 \left(1 - \frac{I_{cr}}{I_g}\right)} \quad (1)$$

where  $I_g$  and  $I_{cr}$  are the gross and cracked moments of inertia, respectively; and  $M_{cr}$  and  $M_a$  are the cracking and applied flexural moments, respectively.

As reported by Bischoff and Gross [27], Eq. (1) provides reasonable estimates of deflections for FRP RC beams and slabs. The factor  $\gamma$  depends on the load and boundary conditions, and implicitly accounts for the length of the uncracked regions of the member. The above authors suggest calculating  $\gamma$  using Eq. (2):

$$\gamma = 1.72 - 0.72 \left(\frac{M_{cr}}{M_a}\right) \quad (2)$$

To predict the deformation of RC beam elements, EC2 [25] includes the effect of tension stiffening based on the CEB-FIP Model Code approach [28, 29]. Accordingly, Eq. (3) is used to calculate the short-term deflection  $\delta$ :

$$\delta = \beta \left(\frac{M_{cr}}{M_a}\right)^m \delta_g + \left[1 - \beta \left(\frac{M_{cr}}{M_a}\right)^m\right] \delta_{cr} \quad (3)$$

In Eq. (3), the deflections in the uncracked ( $\delta_g$ ) and cracked ( $\delta_{cr}$ ) stages are calculated assuming constant uncracked and cracked sectional moments of inertia along the beam, respectively. The recommended values for the coefficients  $\beta$  and  $m$  are 1 and 2, respectively. Al-Sunna et al. [4] proposed the use of Eq. (3) to calculate total deflections of FRP RC

beams, but a value  $\beta=0.5$  was recommended for beams reinforced with Glass FRP (GFRP). Consequently, such value is adopted for the analyses carried out in this study.

More recently, Dundar et al. [23] proposed a more advanced model to calculate deflections of FRP or steel RC elements. The model considers either the a) curvature distribution along the member, or b) effective flexibility models available in the literature. In the cracked state, the model uses a complete moment-curvature relationship obtained from sectional analyses. The model can compute deflections over the full loading history, including post-yielding if reinforcing steel is used. Accordingly, the effective flexibility of the member at a specific section can be expressed as:

$$\frac{1}{E_c I_e} = \frac{1}{E_c I_{cr}} \left[ 1 - \left( 1 - \frac{\varphi_M}{M_a} \right) E_c I_{cr} \right] \leq \frac{1}{E_c I_{cr}} \quad (4)$$

where  $E_c$  is the modulus of elasticity of concrete, and  $\varphi_M$  is the curvature of the member at a value of applied moment  $M_a$ . Due to its versatility, Eq. (4) represents the state-of-the-art for calculating deflections of FRP RC elements.

### 3. Experimental programme

To assess the effect of additional shear deformations, twelve tests were carried out on six beams reinforced with GFRP in flexure and shear. The parameters examined were expected to influence the overall deformation of the specimens, and included different: 1) stirrup strength; 2) shear reinforcement ratio; 3) type of flexural reinforcement, and 4) type of FRP. The beams were designed with sufficient flexural reinforcement in order to induce a shear failure. Different arrangements of shear reinforcement were investigated to assess its effect on the total shear capacity and deformations.

### 3.1. Beam characteristics

Table 1 summarises details of the tested beams and parameters examined in this study. The beam specimens had a rectangular cross-section of 150×250 mm and a total length of 2500 mm. To promote a shear-dominated behaviour, each beam was subjected to four-point bending with a shear span to effective depth ratio ( $a/d$ ) equal to 3.5. Two types of GFRP bars were used as flexural reinforcement. Two  $\phi 16$  mm Sc bars were used in beams TB1 to TB3, thus leading to a flexural reinforcement ratio  $\rho_f = 1.22\%$ , whereas three  $\phi 13.5$  mm Eu bars were used in beams TB4 to TB6 ( $\rho_f = 1.30\%$ ). The reinforcement in the compression zone of all beams consisted of two  $\phi 9$  mm Eu bars. Each shear span (see shear span sides A and B in Fig. 2) was reinforced in shear with internal FRP stirrups at different spacing. Different stirrup spacing was selected for each span in order to test each specimen twice, thus testing a different span at the time. The shear reinforcement ratio  $\rho_w$  of the beams varied between 0.18 and 0.48. In Table 1, the beams are identified using two letters (TB), followed by the specimen number (1 to 6), and a final letter that stands for the tested span side (A or B). Beam TB 6B had no shear reinforcement and was used as a control specimen.

Table 1 Details of reinforcement used in tested beams

Beam ID	Flexural reinforcement				Shear reinforcement		
	Area (mm <sup>2</sup> )	Effective depth (mm)	$\rho_f$ (%)	Bar type	Area (mm <sup>2</sup> )	Spacing (mm)	$\rho_w$ (%)
TB 1A					60	164	0.24
TB 1B					60	164	0.24
TB 2A	402	219	1.22	Sc	60	164	0.24
TB 2B					60	109	0.37
TB 3A					60	98	0.41
TB 3B					60	219	0.18
TB 4A					60	165	0.24
TB 4B					60	110	0.36
TB 5A	429	220	1.30	Eu	60	132	0.30
TB 5B					96	132	0.48
TB 6A					60	165	0.24
TB 6B					No shear reinforcement		

## 3.2. Materials

### 3.2.1 FRP reinforcement

Commercially available pultruded thermoset GFRP bars were used to reinforce the beams in flexure. The  $\phi 16$  mm Sc round bars had a machined threaded surface (Fig. 1a), whereas the  $\phi 13.5$  mm Eu bar had a rough surface produced by peel ply (Fig. 1b). The closed shear stirrups were specially manufactured using two types of thermoplastic GFRP strips (see Fig. 1c). PL stirrups (cross section  $3 \times 10$  mm) were prepreg composites consisting of a thermoplastic polypropylene matrix and continuous unidirectional glass fibres (35% by fibre volume). The Ce stirrup had a similar cross section but consisted of a thermoplastic polypropylene matrix and continuous unidirectional glass fibres (29% by fibre volume). The mechanical properties of the FRP reinforcement used to reinforce the beams in flexure and

shear are listed in Table 2. Such properties were obtained by testing at least three bar or stirrup strip samples in direct tension, as reported in reference [30].

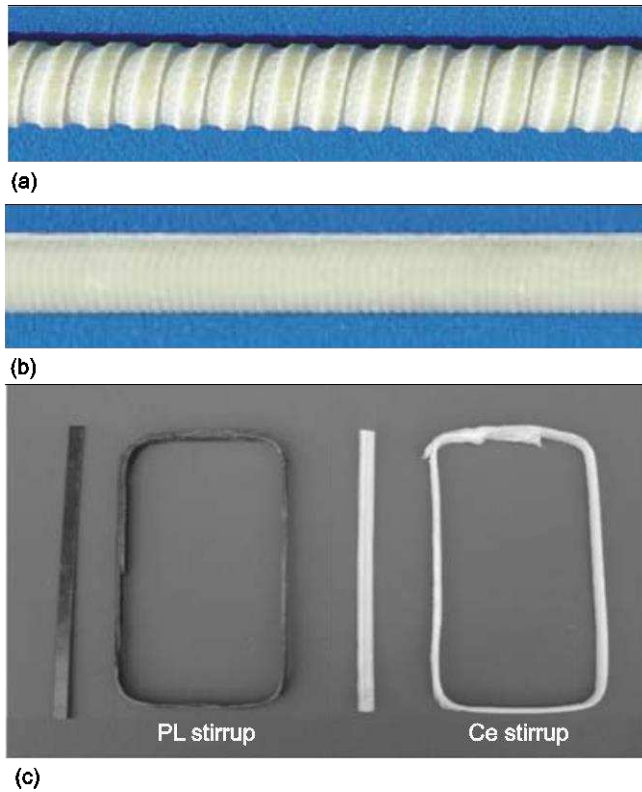


Fig. 1. GFRP reinforcement used: (a) Sc bar, (b) Eu bar, (c) PL strip and (d) Ce strip

Table 2 Mechanical properties of GFRP reinforcements

FRP bars	Cross section (mm)	Modulus of elasticity (GPa)	Ultimate stress (MPa)	Ultimate strain (%)
Sc	$\phi 16$	60	1000	1.8
Eu	$\phi 13.5$	45	700	1.7
PL	3×10	28	720	1.9
Ce	3×10	25	N/A	1.7

### 3.2.2 Concrete

A single batch of ready-mix concrete with a target slump of 50 mm was used to cast the beams. The mix was produced using concrete C50 with 10 mm maximum aggregate size and

Ordinary Portland Cement (OPC) type I. Mean compressive strength values were obtained from 100 mm cubes according to BS EN 12390-3 [31]. The indirect tensile splitting strength ( $f_{ctm}$ ) was determined from tests on six 100×200 mm cylinders according to BS EN 12390-6 [32]. The flexural strength ( $f_{cfm}$ ) was obtained from four-point bending tests on three 100×100×500 mm prisms according to BS EN 12390-5 [33]. All cubes, cylinders and prisms were cast at the same time and cured together with the beams. Table 3 reports the average strength and standard deviations from the tested cylinders and prisms. The mean modulus of elasticity calculated according to EC2 was  $E_{cm}=33.2$  GPa.

Table 3 Properties of concrete for tested beams

	Compressive strength $f_{cm}$	Tensile strength $f_{ctm}$	Flexural strength $f_{cfm}$
Mean (MPa)	60.1	3.60	5.20
Std. Dev. (MPa)	2.56	0.37	0.34
Sample (N <sup>o</sup> )	18	18	9

### 3.3. Experimental set-up and instrumentation

The beams were tested in four-point bending using a 250 kN-capacity servo-controlled actuator and a stiff spreader loading beam, as shown in Fig. 3. The specimens were simply supported over a span of 2300 mm through rollers supported on 100 mm wide steel plates. Equal concentrated loads were applied symmetrically at the beams' mid-span to produce a constant moment in this region. All tests were performed in displacement control and the evolution of damage (crack pattern and crack widths) was monitored at load increments of 5 or 10 kN using a hand held micrometer. Crack widths were measured at the soffit of the beams in all tests. The load was initially applied up to 40 kN and then removed to relief possible residual strains (which would lead to spurious strain gauge readings), and to check

the instrumentation and data acquisition system. Subsequently, the specimens were reloaded to induce strains in the flexural and shear reinforcement of approximately 4500-5000  $\mu\epsilon$ . Foil-type strain-gauges were bonded at various locations (see Fig. 2) along the flexural and shear reinforcement to monitor strain. Most gauges were fixed on the flexural reinforcement within the shear spans to measure the effect of shear cracks. Strain gauges were also fixed at the mid-span and under the point loads. In addition, strain gauges were also attached on selected shear stirrups to capture the strain values produced by diagonal shear cracks. All beams were subjected to two consecutive tests, one on each span side. In all specimens, side A was tested first. To prevent excessive cracks or failure during the initial test on side A, side B of all beams was externally confined using post-tensioned steel straps [34], as shown in Fig. 3. After the test on side A was halted, the straps were removed from side B, new straps were fixed on side A, and side B was retested to produce shear failure of the specimen.

The beam deflections were measured at each load increment using Linear Variable Differential Transducers (LVDTs) situated at the mid-span, under the point loads and at every 256 mm under the shear span (see Fig. 2). Two additional LVDTs at the top-face of the beam supports measured deflections at the supports, thus enabling the calculation of the net beam deflections.

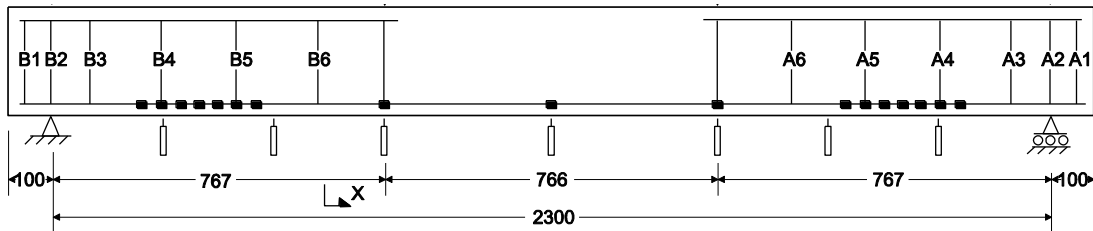
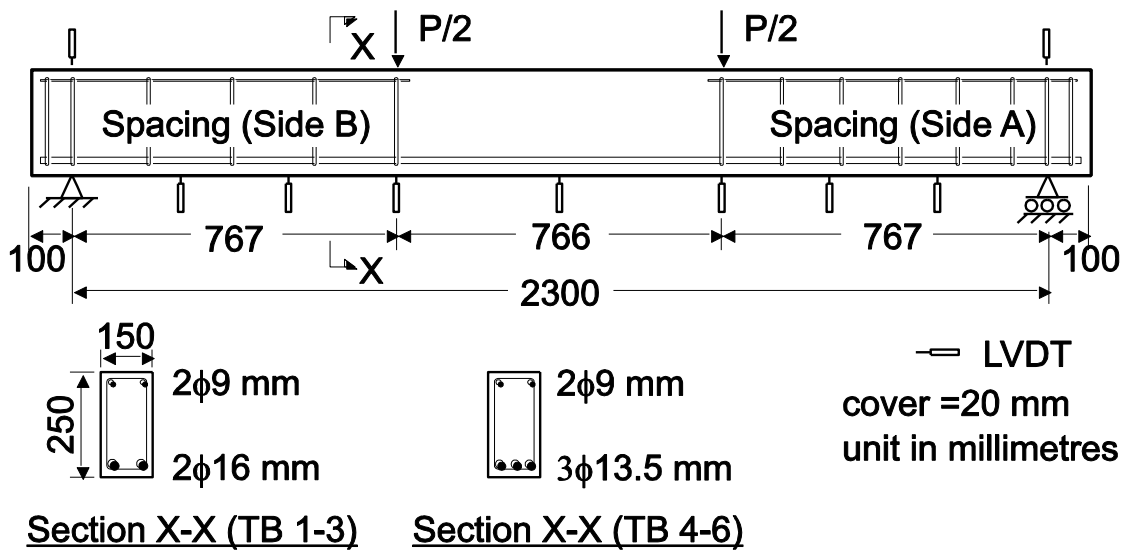


Fig. 2. Test set-up and location of strain gauges and LVDTs



Fig. 3. Typical view of beams during tests and pre-tensioned steel straps on side B (TB 1)

## 4. Test results and analysis

Table 4 summarises the experimental results in terms of diagonal cracking load ( $P_{cr}$ ), ultimate load at failure ( $P_u$ ), maximum deflection at mid-span ( $\delta_{max}$ ), maximum flexural crack width ( $w_1$  at mid-span), major diagonal shear cracks observed during the tests ( $w_2$ - $w_4$ ), and average crack spacing. The following sections summarise the most significant observations of the testing programme and discuss the results listed in Table 4.

Table 4 Summary of experimental results

Beam ID	$P_{cr}$ (kN)	$P_u$ (kN)	$\delta_{max}$ (mm)	$w_1$ at load P (mm)	Major diagonal shear cracks (mm)			Average crack spacing (mm)
					$w_2$	$w_3$	$w_4$	
TB 1A	63.8	70.2	21.0	0.40@70	0.25	-	-	70
TB 1B	64.4	79.1	20.5	0.35@60	0.10	0.05	0.08	-
TB 2A	69.4	72.0	21.1	0.45@70	0.05	0.10	0.01	77
TB 2B	66.5	131.4	41.2	0.50@80	0.20	0.20	0.10	-
TB 3A	72.8	126.4	37.7	0.40@80	0.10	-	-	77
TB 3B	60.4	76.8	24.3	0.25@60	0.30	0.60	0.80	-
TB 4A	53.0	65.6	22.4	0.35@60	0.20	0.35	0.02	85
TB 4B	65.0	118.6	45.4	0.35@60	0.25	0.20	0.02	-
TB 5A	55.8	133.7	36.6	0.50@60	0.20	0.20	0.05	85
TB 5B	72.7	133.7	48.2	0.45@60	0.70	0.60	0.05	-
TB 6A	57.0	61.2	18.8	0.28@60	0.18	0.20	0.08	85
TB 6B	58.1	58.1	16.8	0.29@50	0.20	0.22	0.10	-

### 4.1. Shear capacity and observed failure

The test on side A of the beams with stirrups was halted when strain levels in both flexural and shear reinforcements exceeded a critical value of 4500-5000  $\mu\epsilon$ . It was assumed that, at such strain levels, the load recorded was close to the ultimate capacity ( $P_u$ ) of the tested shear span as observed in similar beams tested by Guadagnini et al. [5,6]. On the other hand, the

diagonal cracking load ( $P_{cr}$ ) was experimentally determined as the load at the onset of diagonal cracking.  $P_{cr}$  was assumed to be the load at which the FRP stirrups were fully mobilised, as evidenced by a sudden increase of strains in the shear stirrups.

The crack development was similar for all beams. The initial load formed small flexural cracks within the mid-span and shear span regions; these cracks became wider and visible to the naked eye as the load increased. Major shear cracks (i.e.  $w_{2A}$ ,  $w_{3A}$ , and  $w_{4A}$ ) were observed in all beams (see for example Fig. 4a) as the load increased further. The maximum loads varied from 61 to 126 kN, depending predominantly on the shear reinforcement ratio in span A. It should be noted that the actual capacity of side A of the beams may be slightly higher had the tests been continued up to failure; as a result, the values reported in Table 4 are slightly conservative.

During the tests on side A, several shear cracks developed on side B but crack opening was effectively controlled (maximum width=0.01 mm) by the post-tensioned steel strapping around the latter side. During the tests on side B, the flexural and shear cracks developed during the tests in side A propagated and penetrated deeper towards the loading point as the applied load increased. After the formation of diagonal cracks, the strain recorded in the shear stirrups increased rapidly and, eventually, failure occurred. As expected, all beams with stirrups were dominated by a shear diagonal failure. This was accompanied by stirrup rupture and concrete spalling at the beams' soffit (Fig. 4b,c). The measured ultimate capacities of the beams with stirrups ranged between 77 and 134 kN.

Unlike the beams reinforced with shear stirrups, the control specimen without stirrups (TB 6B) did not develop new diagonal cracks during the tests on side B. During testing, the existing shear cracks widened further and propagated towards the loading point. Failure occurred at a load of 58 kN due to excessive widening of a diagonal crack (labelled as  $W_{3B}$  in Fig. 4d) that formed during the initial test on side A. Note that, for side B of the beams,  $P_{cr}$

was also assumed as the load at which the FRP stirrups were fully mobilised, as evidenced by a sharp increase of strains in the shear stirrups.

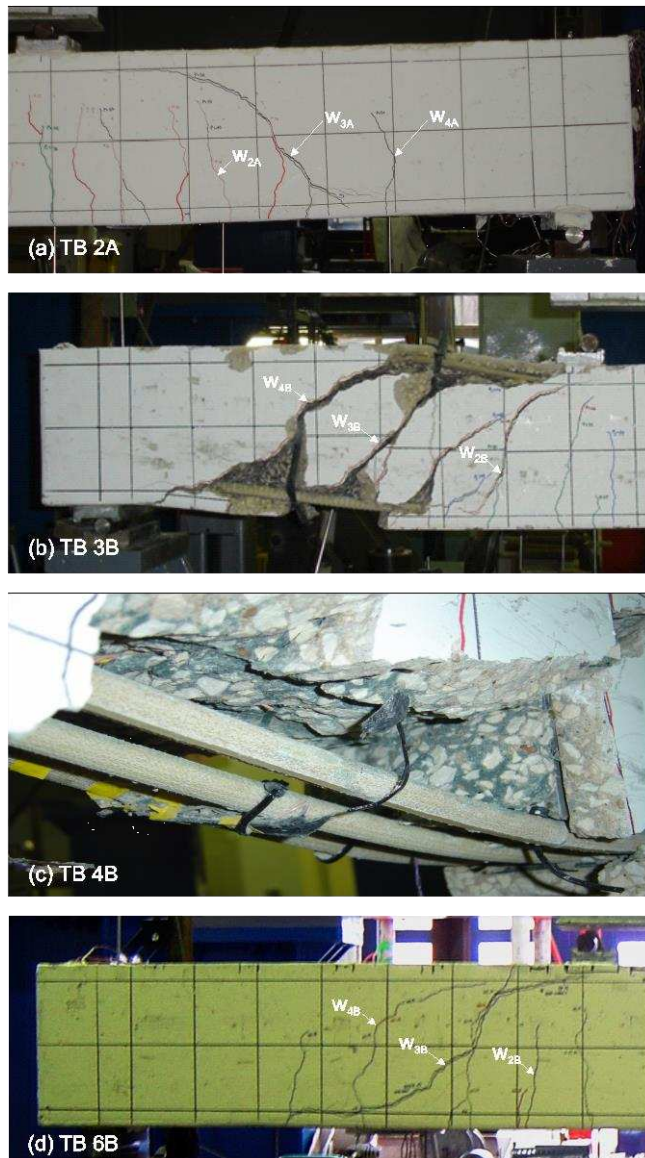
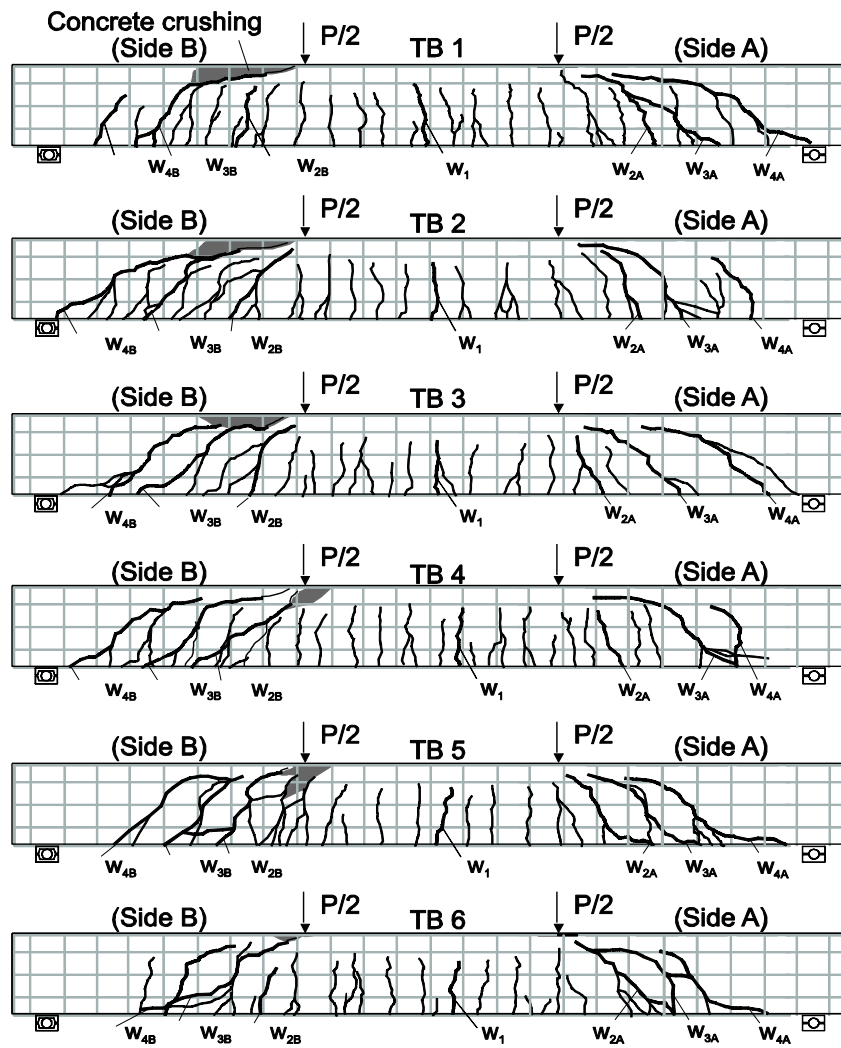


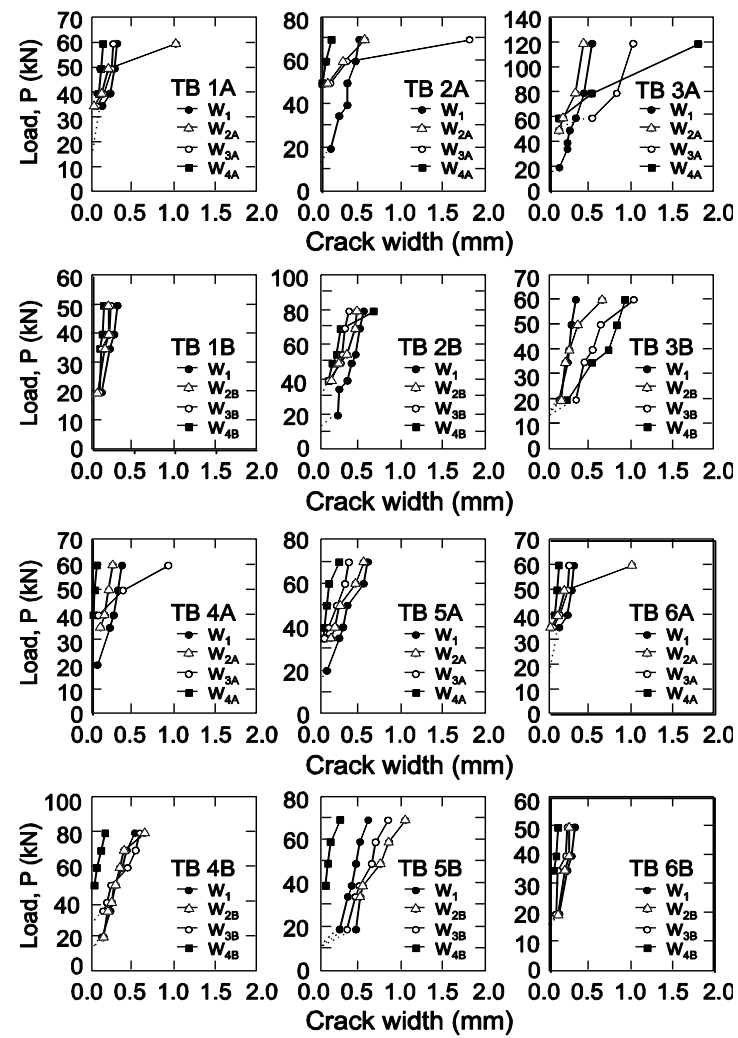
Fig. 4. Diagonal tension failure of beams: (a) TB 2A, (b) TB 3B; (c) stirrup rupture in the bent region (TB 4B), and (d) view of beam TB 6B during testing

Fig. 5a shows the crack pattern observed during the tests, whereas Fig. 5b shows the measured crack widths at different load levels. In general, at maximum load (see Table 4), more cracks appeared in beams reinforced with bars Sc (beams TB 1 to TB 3) than in beams

reinforced with bars Eu (beams TB 4 to TB 6). Moreover, the average crack spacing was 10% higher in the latter beams. The larger number of cracks in beams with Sc bars can be attributed to a more distributed bond stress along such bars. Note that the crack spacing reported in Table 4 is an average value obtained by dividing the length of the constant moment zone by the total number of cracks at maximum load on side A.



(a)



(b)

Fig. 5. (a) Final crack pattern of beam specimens after tests, and (b) measured crack width of beam specimens

## 4.2. Strain in flexural and shear reinforcements

Fig. 6 shows the strains recorded along the flexural reinforcement of beam TB 3B, which is representative of the rest of the specimens. For clarity, the results are presented at load intervals of approximately 10 kN and only up to the peak load. As expected, large strains were recorded at mid-span as a result of the flexural cracking produced by increasing loads. The sharp increase of longitudinal bar strains at 60 kN (see side B in Fig. 6) was due to the development of shear cracks. In all beams, strains measured in the longitudinal reinforcement always exceeded 0.5% at maximum load.

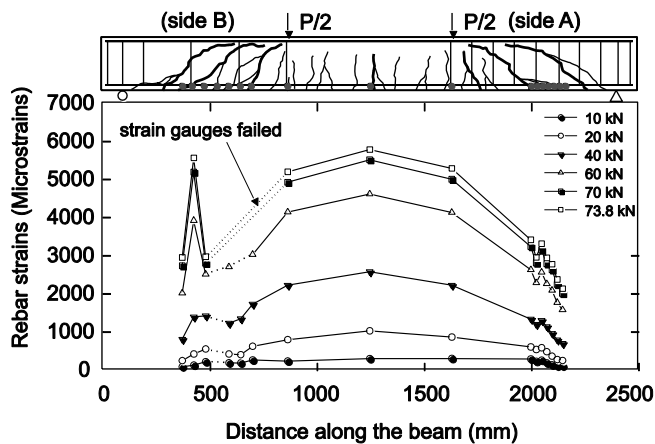


Fig. 6. Longitudinal bar strains recorded during the test on beam TB 3B

Fig. 7 shows the variation of strains in the shear reinforcement of beam TB 1. The stirrups A3-A6 shown in this figure were located on side A of the beam, while stirrups B3-B6 were on side B. It is shown that, for both beam sides, the measured strains increased rapidly after the formation of diagonal cracks at 65 kN. The load at the onset of diagonal cracking was well captured by several strain gauges in at least two shear stirrups. Once the diagonal cracks formed, the strain gauges adjacent to the cracks were mobilised and the strains increased rapidly up to beam failure. Fig. 7 also shows that i) the distribution of strain along the stirrups was not uniform (e.g. stirrups A4, A5, B4, B5), and ii) higher strains were recorded at strain

gauges adjacent to the cracks. The crack development and strain gauge readings are used in the following section to derive a practical model for predicting the deflections of FRP RC beams.

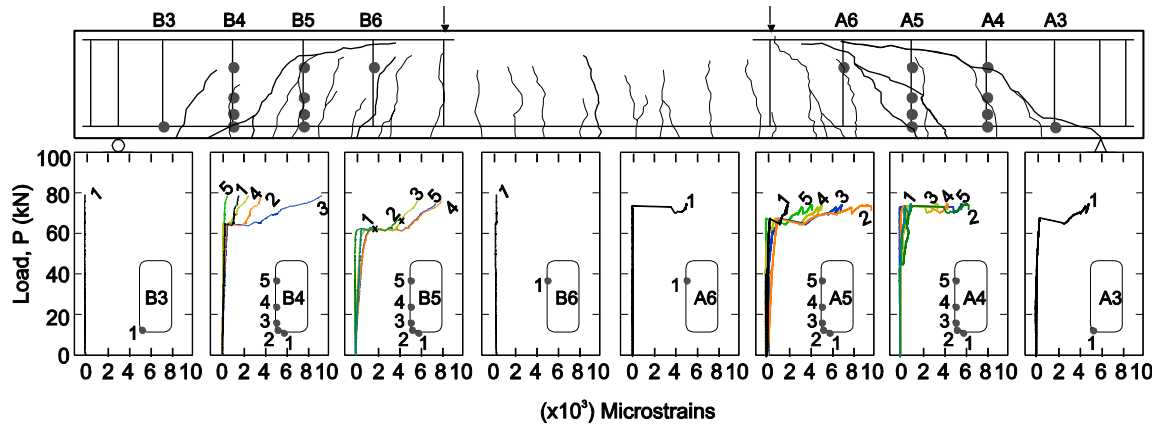


Fig. 7. Final crack pattern of beam TB 1, location of strain gauges (dots) and corresponding strain distribution in shear stirrups

### 4.3. Analysis of beam deflections

#### 4.4. Theoretical predictions vs experimental results

The total mid-span deflection,  $\Delta_{mid}$ , of the tested beams subjected to bending and shear can be obtained using virtual work principles:

$$\Delta_{mid} = \frac{23PL^3}{1296EI} + \frac{\phi PL}{6GA} \quad (5)$$

where  $P$  is the total load,  $L$  is the clear span of the beam,  $\phi$  is the form factor ( $\phi = 6/5$  for a rectangular section),  $I$  is the moment of inertia,  $A$  is the cross sectional area of the beam, and  $E$  and  $G$  are elastic and shear modulus, respectively ( $G = E/2(1 + \nu)$ ).

For RC elements, the effective moment of inertia  $I_{ef}$  is often used to calculate the flexural deformation component (first term on right hand side of Eq. 5), whereas the shear component (second term of Eq. 5) is considered negligible for slender beams. Shear deformations are not

explicitly accounted for in ACI 318 [35] nor in Model Code [28, 29] models for calculating deflections of RC beams or slabs. Nevertheless, the CEB 158 [36] guidelines consider shear deformations of RC members by defining two states of shear strains, as shown in Fig. 8. In this figure, the magnitude of shear strains largely depends on the formation of inclined shear cracks. If no shear cracks occur (i.e.  $V < V_r$ , where  $V_r$  is the shear cracking force in state I, Fig. 8), the shear deformations are elastic, very small and can be thus neglected. However, after the development of inclined cracks ( $V_r < V < 4V_r$ , state II in Fig. 8), shear deformations are significant. In this case the calculation of the overall shear deformation uses a parabolic function from the elastic shear deflection to the fully opened shear crack deflection due to shear.

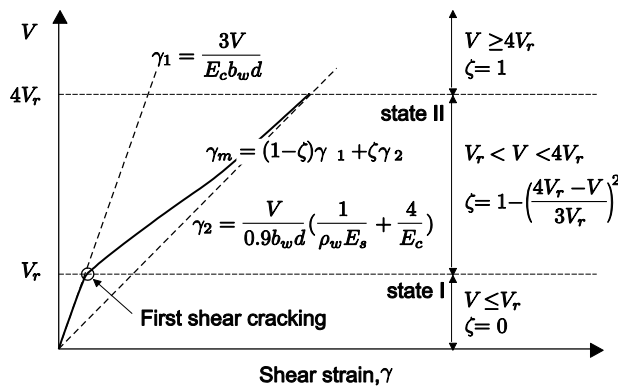


Fig. 8. Shear strain as a function of applied shear force (adapted from CEB 158)

Accordingly, CEB 158 [36] calculates the shear cracking force  $V_r$  as:

$$V_r = \tau_r k (1 + 50 \rho_l) b_w d \quad (6)$$

where the shear stress  $\tau_r$  depends on the concrete strength (refer to Table 3.5.1 of the CEB 158, 1985),  $k=1.6-d$  with  $d$  in meters, and  $\rho_l$  is the longitudinal reinforcement ratio ( $A_s / b_w d$ ).

Figs. 9 and 10 compare the load-deflection responses from side A of the tested beams with a) the flexural deflection predictions ( $\delta_f$ ) calculated according to EC2 but ignoring the shear deflection, and b) deflections according to EC2 ( $\delta_f$ ) plus the shear deflection given by CEB 158 ( $\delta_s$ ). Likewise, the figures also compare the load-deflection response from side B of the beams with the predictions given by cracked section analysis (CSA). It should be noted that the concrete tensile strength used to determine the cracking moment and cracking load was derived from inverse analysis to account indirectly for the variability of concrete, size effect, and shrinkage effects on the initial strain state within the element and on the apparent concrete properties [37].

Overall, the results in Figs. 9 and 10 indicate that the analytical models predict reasonably well the deflections up to (low) loads corresponding to service conditions. In this study, the service load is assumed to be about 35% the nominal moment capacity of beams TB 1-3 and TB 4-6, which corresponds to loads of 55 and 50 kN, respectively. However, the predictions given by the models underestimate considerably deflections at higher loads (i.e. after diagonal cracking). Such inconsistencies are attributed to the formation of shear diagonal cracks at higher load levels, which results in an additional deformation component. This component is referred to as shear crack induced deformation in subsequent sections of this study. Note that the load at shear diagonal cracking ( $P_{cr}$ ) can be determined experimentally from strains in the stirrups, as these are mobilised only upon the occurrence of diagonal cracking (see Table 4).

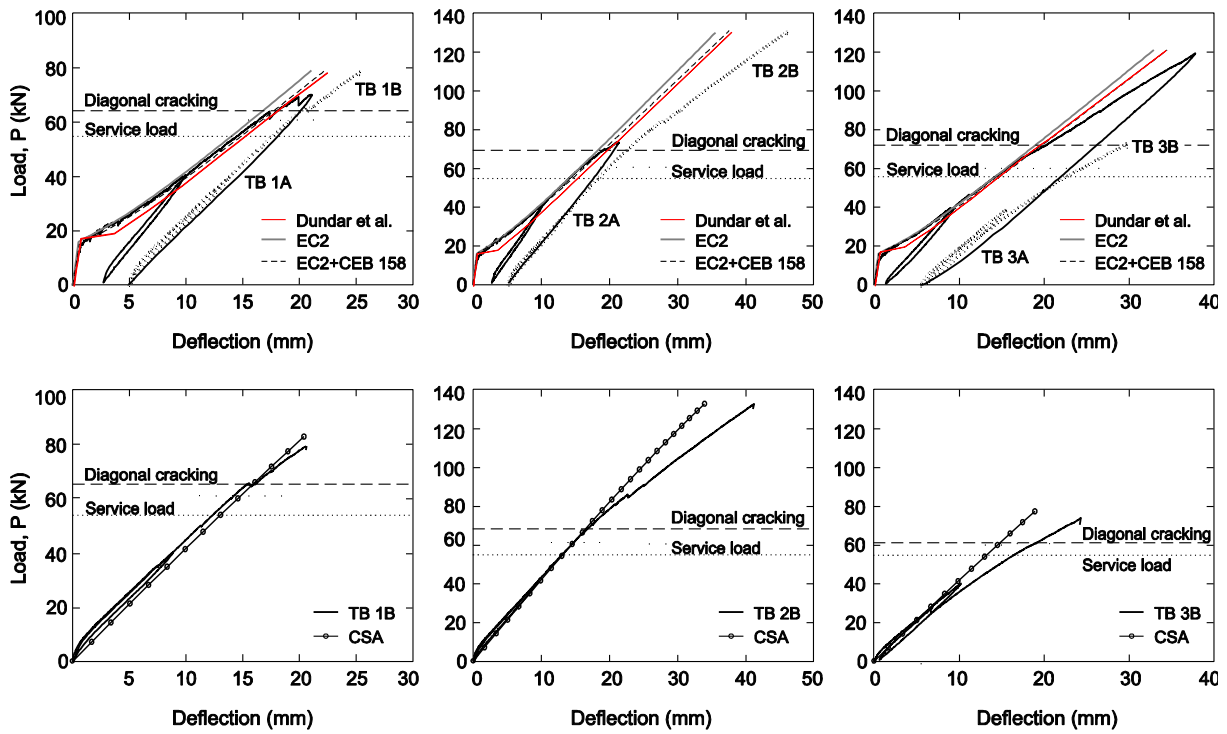


Fig. 9. Comparison of the mid-span deflection between test results and theoretical predictions (beams TB 1-3)

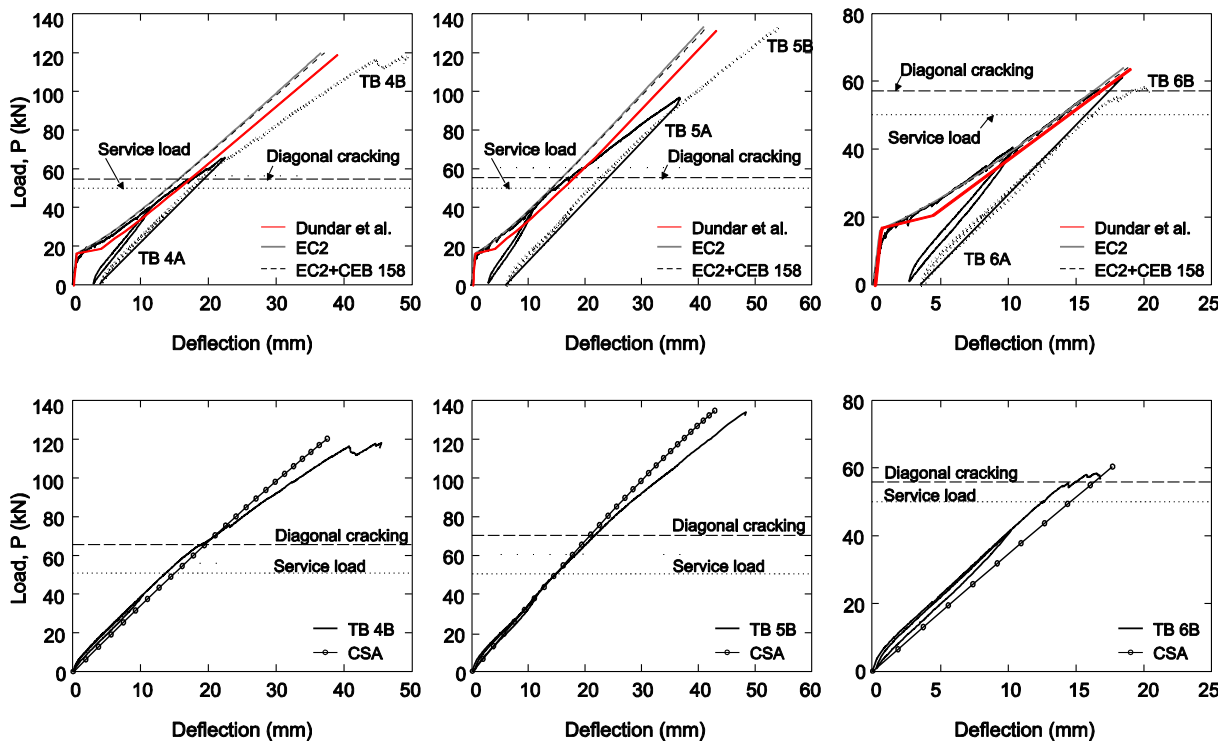


Fig. 10. Comparison of the mid-span deflection between test results and theoretical predictions (beams TB 4-6)

#### 4.4.1 Effect of flexural reinforcement stiffness

To investigate the effect of longitudinal reinforcement on the additional shear crack induced deflections, the deflections from the tests on side B are compared to analytical predictions obtained using CSA, but ignoring the concrete contribution in tension. The effect of different longitudinal reinforcement on shear deformation can be examined from the results of TB 2B and TB 4B, which had longitudinal reinforcement ratios of 1.22% and 1.33%, respectively. Fig. 11 shows that, at equivalent load levels, TB 2B had lower additional deflection (i.e.  $\Delta\delta$  in shaded region) than TB 4B. This is due to the higher flexural reinforcement stiffness  $E_f \rho_f$  of bar Sc (0.732) compared to bar Eu (0.598), which resulted in less axial deformation in the bar and thus reduces both flexural and shear deformations.

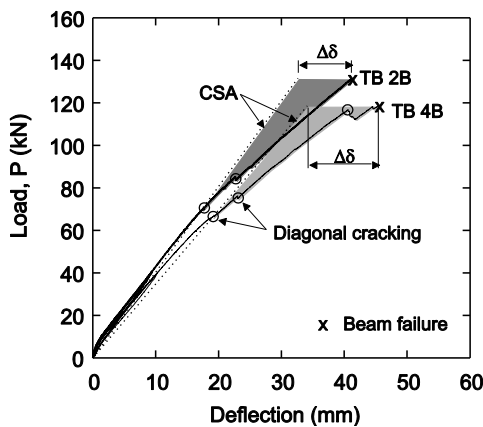


Fig. 11. Effect of longitudinal reinforcement content on beam deflection.

#### 4.4.2 Effect of shear reinforcement ratio

Fig. 12 compares the load-deflection response of beams TB 4B, TB 5B and TB 6B. These beams had the same longitudinal reinforcement, but the shear reinforcement ratios of specimens TB 4B and TB 5B were 0.36% and 0.48% respectively, whereas specimen TB 6B had no shear reinforcement. The results in Fig. 12 show that TB 6B had a capacity of only 58 kN at 16.8 mm. The total deflections of TB 4B and TB 5B were similar after the diagonal crack formed (at 65 kN and 73 kN, respectively, as determined from stirrup strains) and up to

a load of 110 kN. At this load, another diagonal crack developed in beam TB 4B, thus increasing rapidly the overall deflection. At ultimate load, the shear deformation of specimens TB 5B and TB 4B accounted for 20% and 30% of the total beam deformation, respectively.

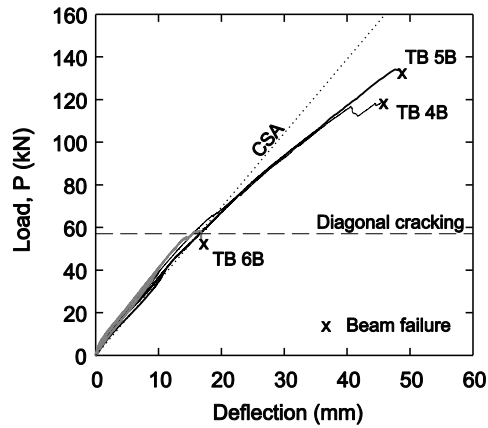


Fig. 12. Effect of shear reinforcement ratio on beam deflection.

Based on the analysis of the beam deflection, it is evident that the contribution of crack induced deformations to the total deflection of FRP RC beams can be significant. The additional deflection due to shear crack opening can be added to existing predictive equations for calculating overall beam deformations up to failure. The following section proposes a practical semi-empirical model that can be incorporated into existing code equations for calculating accurately overall beam deformations up to failure.

## 5. Model proposal for estimating shear crack induced deflections

The proposed model considers an element of an RC beam subjected to bending and shear, as shown in Fig. 13. The total deformation of the element,  $\delta_{tot}$ , is assumed to have deformation components due to pure bending  $\delta_f$  (Fig. 13a), pure shear  $\delta_s$  (Fig. 13b), and rigid-body movement  $\delta_R$ , accordingly:

$$\delta_{tot} = \delta_f + \delta_s + \delta_R \quad (7)$$

$\delta_R$  can be further decomposed into global rigid movement,  $\delta_{Ra}$  (Fig. 13c), and localised rigid body movement due to the formation of macro cracks,  $\delta_{Rcr}$  (Fig. 13d).

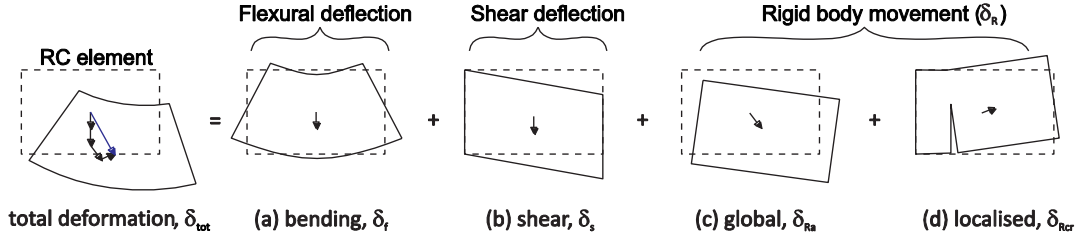


Fig. 13. Decomposition of the total deflection of a RC element subjected to bending and shear force

The value of  $\delta_s$  is generally negligible in slender RC elements. However, when diagonal shear cracks develop, the additional localised rigid body deformation  $\delta_{Rcr}$  (due to crack opening) can be significant. This component of deformation can be determined considering the change in geometry of the beam element as a rigid body rotation around the tip of a macro crack, as shown in Fig. 14 for a beam subjected to two-point loads. If the horizontal movement and support settlement are ignored, the value of the angle  $\alpha$  is defined as the sum of the angles  $\beta_1$  and  $\beta_2$ , i.e:

$$\alpha = \beta_1 + \beta_2 \quad (8)$$

For very small angles  $\beta_1$  and  $\beta_2$ , the following geometrical relationships can be established:

$$\beta_1 \approx \frac{x}{l_1} \approx \frac{\delta_{cr}}{(L/2)} \quad (9)$$

$$\beta_2 \approx \frac{x}{l_2} \approx \frac{\delta_{cr} l_1}{l_2(L/2)} \quad (10)$$

Substituting Eqs. (8) and (9) into Eq. (7) and rearranging terms, the mid-span deflection can be defined as:

$$\delta_{cr} = \frac{\alpha(L/2)}{1 + (l_1/l_2)} \quad (11)$$

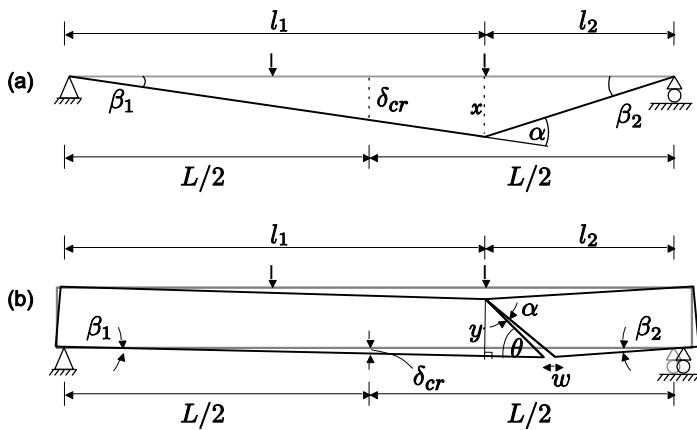


Fig. 14. Single straight shear crack model

The angle  $\alpha$  can be expressed as a function of the crack width  $w$ , and the height of the crack tip  $y$ . It should be noted that, in practice, several cracks can develop within the shear span of a RC beam. Whilst these shear cracks always initiate vertically (usually as progression of previous flexural cracks), their orientation changes rapidly as a result of the change in direction of the principal stresses. Fig. 15a shows a possible distribution of idealised curved shear cracks along the shear span of a RC beam, whereas Fig. 15b shows idealised straight diagonal cracks that represent the inclination of the curved cracks.

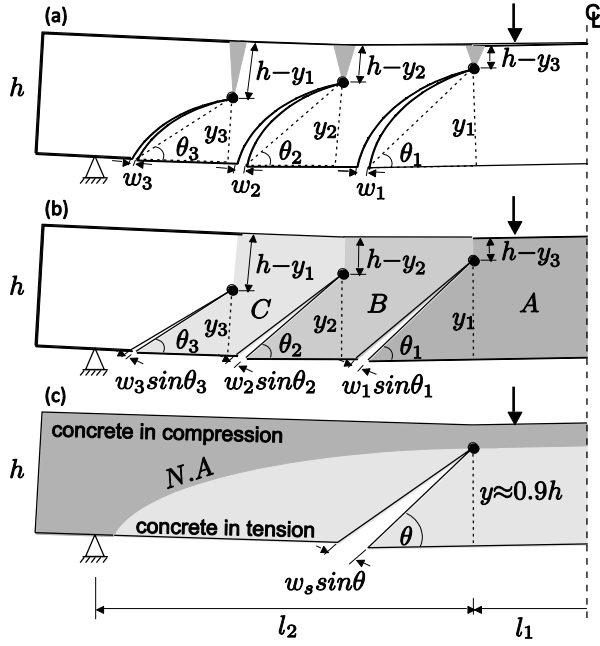


Fig. 15. Idealised shear cracks in a concrete beam element

Thus, the maximum deflections at mid-span due to the rigid-body movement of the beam can be obtained by adding the deflections of each of the elements between cracks (elements A, B and C in Fig. 15b). For simplicity, it is assumed that the mid-span deflection  $\delta_{cr}$  can be calculated using a fictitious single diagonal crack with a total width equal to the sum of all the developed shear cracks (Fig. 15c) according to Eq. (12):

$$\delta_{cr} = \sum \left[ \frac{w_s \sin \theta}{y} \right] \cdot \left[ \frac{L/2}{1 + (l_1/l_2)} \right] \quad (12)$$

where  $w_s$  is the sum of the shear crack widths;  $\theta$  is the inclination of the single crack;  $y$  is height of the crack tip;  $L$  is the total span of the beam ( $L=l_1+l_2$ ); note that  $l_1$ ,  $l_2$  and  $y$  indicates the location of the crack tip from each support (see Fig. 15c). Eq. (12) indicates that the additional component of deflection caused by the formation of shear diagonal cracks is a function of 1) the crack width  $w$ , 2) the inclination angle of the crack  $\theta$ , and 3) the location of the crack tip with reference to the support. The effect of these parameters is examined in more detail through a sensitivity analysis.

## 5.1. Sensitivity analysis

Eq. (12) was used to assess the additional component of deflection from shear diagonal cracks on the tested beam specimens. Different values of crack inclination (starting from  $\theta=21.8^\circ$ ) were used to study their effect on the beam deflection results, including a simplified analysis assuming a fixed crack angle ( $\theta=45^\circ$ ). Fig. 16 compares the additional mid-span deflection for the tested beams. The results show that a fixed crack angle ( $\theta=45^\circ$ ) leads to a higher mid-span deflection with an increase in the crack width and its inclination angle. As shown later, the use of  $\theta=45^\circ$  in the calculations leads to accurate estimations of the additional deflection component due to shear cracks.

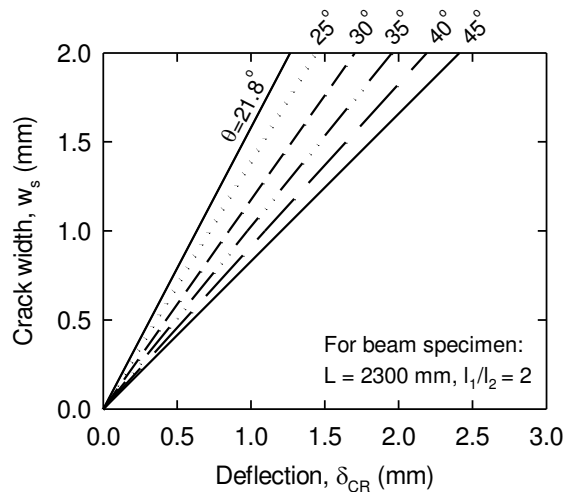


Fig. 16. Effect of variation inclination angle  $\theta$  on beam deflection

In real beams, shear diagonal cracks develop vertically at the beginning of loading. Subsequently, the cracks tend to propagate and penetrate deeper towards the loading points, and finally the cracks' tip stops close to the neutral axis. Conversely, Eq. (12) was derived assuming that the crack tip is at the loading point. For practical purposes, the height of the crack tip can be taken as  $y=0.9h$ , where  $h$  is the total height of the beam.

The proposed model (Eq. (12)) also assumes that several shear cracks can form in the shear span, and that all these cracks contribute to the additional mid-span deflection. However, the location of the actual crack tips is unknown and is difficult to measure in practice. As a result, Eq. (12) can be further simplified assuming that a crack tip occurs very close to the loading point within the shear span (defined as  $a$ ). The horizontal distance of the fictitious crack tip ( $l_2$ ) to the support can be defined as approximately equal to the shear span  $a$ . Assuming  $\theta=45^\circ$  and  $y=0.9h$ , Eq. (12) can be re-written as:

$$\delta_{cr} = \left( \frac{w_s \sin \theta}{2} \right) \cdot \left( \frac{a}{y} \right) \quad (13)$$

Or further simplified for the beams tested in this study:

$$\delta_{cr} = 0.393 w_s \left( \frac{a}{h} \right) \quad (14)$$

It should be noted that the assumptions regarding the number of inclined cracks and the crack angle used in the proposed model may not apply for all load configurations, and thus further research should investigate/extend the applicability of the model to different load cases such as distributed loading or single point loading. It should be also mentioned that the additional deflections computed by Eq. (12) are expected to be conservative for shorter spans or deep beams (i.e. shear cracks are likely to develop at service conditions). For longer spans, the moment-to-shear ratio increases and the contribution of shear deformations to the total deformation is small [38]. As such, Eq. (13) is sufficiently accurate to estimate the additional deflection due to shear cracks in the case of three- and four-point flexural bending using the experimental cracking moment. If the experimental cracking moment is not available, alternative methods such as a strain control approach could be used to estimate the shear crack width, as explained later in section 5.2.

## 5.2. Comparison of theoretical and experimental results

To assess the accuracy of the proposed model, the results from shear diagonal crack development of the tested beams are used (refer to Fig. 5). Only major diagonal cracks were considered in the assessment based on the experimental observations. Moreover, a fixed crack angle  $\theta=45^\circ$  was assumed in the analysis. Figs. 17 and 18 compare the theoretical and experimental load-deflection responses for beam specimens TB 3A and TB 4A, respectively. These are typical results and the following observations apply to the rest of the beams. Three analytical predictions are shown in the figures: a)  $\delta_f + \delta_s$  is the beam deflection considering flexure predictions from EC2 and shear predictions from CEB 158, b)  $\delta_f + \delta_s + \delta_{RCR}$  is the prediction considering the above components plus the additional shear crack induced deflection (i.e. Eq. (13), and c) Dundar et al.'s model using moment-curvature analysis. It is shown that code equations and Dundar et al.'s model predict well the experimental results only before diagonal cracking occurs. In particular, the load-deflection curves obtained from Dundar et al.'s model are closer to the experimental curves of TB 3A and TB 4A compared to the code predictions, which have a stiffer response. Whilst Dundar et al.'s model matches the experimental curves of the tested beams up to approximately 70-80% of their capacity, the deflection calculated by the new proposed model matches well the test results up to ultimate load. However, further comparisons with different test data are necessary to validate the better accuracy of the predictions yield by the proposed model.

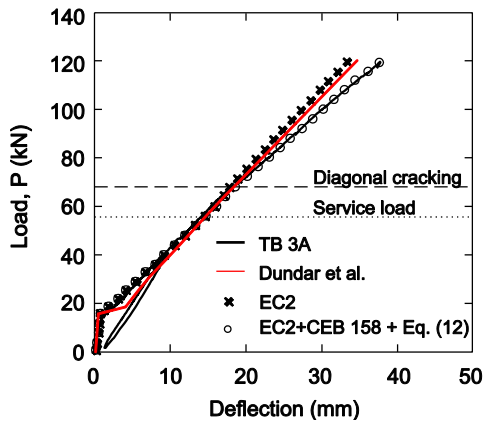


Fig. 17. Prediction of mid-span deflection for specimen TB 3A

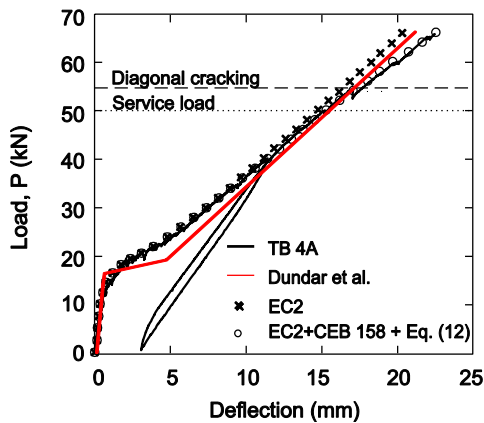


Fig. 18. Prediction of mid-span deflection for specimen TB 4A

Table 5 compares the experimental deflections and the analytical predictions by ACI 440 [24], EC2 [25], Dundar et al.'s model [23] and the proposed model (Eq. 13) for the tests on beam sides A. The results in Table 5 indicate that, compared to the predictions given by existing design guidelines and the advanced moment-curvature approach, the proposed equation predicts the test results more accurately (mean Test/Prediction ratios  $T/P=1.03$  and  $1.02$  at  $P_{cr}$  and  $P_u$ , respectively) and with less scatter (Standard Deviations  $SD=0.03$  and  $0.02$  at  $0.02$  at  $P_{cr}$  and  $P_u$ , respectively). The results in Table 6 confirms that the proposed model also predicts more accurately the experimental deflections on side B of the beams ( $T/P=1.13$  and  $SD=0.07$ ) when compared to CSA. Consequently, it is proposed to use Eq. (13) (or the

more general Eq. 12) to predict the deflection of FRP beams. It should be mentioned that, in real situations, shear crack widths are not easy to determine beforehand. Moreover, the experimental studies available in the literature rarely report detailed data on the progression of shear cracking during tests. In the absence of these data, the designer can, for instance, estimate the additional deformation due to shear action by the strain approach and considering the number of shear stirrups likely to contribute to a beam's shear resistance along with a predetermined limiting strain value such as that proposed for the design of shear stirrups (for example 0.45% [38]). In an attempt to provide a simple design tool, additional shear crack induced deformations could be estimated according to the proposed strain approach which is suitable for design procedure. Such approach will be presented by the authors in a forthcoming article.

Table 5 Experiment and calculated deflections of beams, sides A

Specimen	Deflection at $P_{cr}$ (mm)					Deflection at $P_u$ (mm)				
	Test	ACI 440	EC2	Dundar et al.	$\delta_f + \delta_s + \delta_{CR}$	Test	ACI 440	EC2	Dundar et al.	$\delta_f + \delta_s + \delta_{CR}$
TB 1A	17.6	15.3	16.1	16.3	16.5	21.0	16.7	18.9	19.2	20.2
TB 2A	19.1	16.3	17.1	17.8	18.4	21.1	17.5	19.7	20.1	20.3
TB 3A	18.5	16.1	17.3	17.9	17.5	37.7	28.9	32.6	34.1	37.2
TB 4A	17.2	15.9	16.2	16.9	17.1	22.4	18.3	19.5	21.4	22.1
TB 5A	16.7	15.1	15.9	16.8	16.3	36.6	28.6	29.7	31.9	35.4
TB 6A	15.8	15.1	15.3	15.7	15.8	18.8	16.9	18.3	18.5	18.7
Avg. (T/P)	-	1.12	1.07	1.07	1.03	-	1.23	1.12	1.08	1.02
SD	-	0.05	0.03	0.03	0.03	-	0.07	0.07	0.05	0.02

Note: SD is the standard deviation.

Table 6 Experiment and calculated deflections of beams, sides B

Specimen	Deflection at $P_u$ (mm)		
	Test	CSA	CSA+ $\delta_{CR}$
TB 1B	21.1	19.2	19.6
TB 2B	41.2	34.1	34.8

TB 3B	24.3	18.0	20.5
TB 4B	44.8	36.5	37.2
TB 5B	48.2	42.8	43.0
TB 6B	16.8	16.0	16.5
Avg. (T/P)	-	1.18	1.13
SD	-	0.11	0.07

Note: SD is the standard deviation.

## 6. Conclusions

This study proposes a practical semi-empirical method for determining additional deformation due to shear cracking in FRP RC beams. To account for the contribution of shear cracking to total beam deflection, the model uses a single fictitious inclined crack with a width equal to the sum of the individual effective shear crack widths. The additional deflection obtained by the proposed model can be added to the deflection predicted by CSA or by equations in existing design guidelines. Based on the results of this study, the following conclusions are drawn:

- The deflection of FRP RC beams can be adequately predicted by equations included in current guidelines (e.g. ACI 440, EC2) and the advanced moment-curvature model by Dundar et al. but only up to the service limit. At higher load levels, such equations can significantly underestimate deflections by up to 30%.
- The experimental results indicate that the additional component of deflection due to shear crack development needs to be added to the components due to bending and rigid-body movement. The results also show that diagonal cracking can occur even under normal service conditions and can rapidly increase the magnitude of the overall deflection.
- The estimated total deflection of FRP RC members can be significantly improved by adding the component of deflection due to shear action and crack opening to the flexural deflection calculated by existing predictive equations. Compared to ACI 440 and EC2,

the proposed model provides more consistent predictions and less scatter up to beam failure.

## Acknowledgements

The first author thankfully acknowledges the financial support from the National Research Council of Thailand (Contract N<sup>o</sup>. 901/2559) and the Rajamangala University of Technology Tawan-Ok. The analytical work and model development were carried out at the University of Sheffield under the Newton-Fund Research Travel Grant programme (2015).

## References

- [1] Shehata E, Morphy R, Rizkalla S. Fiber reinforced polymer shear reinforcement for concrete members: Behavior and design guidelines. *Canadian Journal of Civil Engineering* 2000;27:859–72.
- [2] Hansapinyo C, Pimanmas A, Maekawa K, Chaisomphob T. Proposed Model of Shear Deformation of Reinforced Concrete Beam After Diagonal Cracking. *Journal of Materials, Concrete, Structures and Pavements, JSCE* 2003;58:305-19.
- [3] Ueda T, Sato Y, Ito T, Nishizono K. Shear Deformation of Reinforced Concrete Beam. *Journal of Materials, Concrete, Structures and Pavements, JSCE* 2002;56:205-15.
- [4] Al-Sunna R, Pilakoutas K, Hajirasouliha I, Guadagnini M. Deflection behaviour of FRP reinforced concrete beams and slabs: an experimental investigation. *Composites Part B: Engineering* 2012;43:2125-34.
- [5] Li A, Diagana C, Delmas Y. CRFP contribution to shear capacity of strengthened RC beams. *Engineering Structures* 2001;23:1212-20.
- [6] Diagana C, Li A, Gedalia B, Delmas Y. Shear strengthening effectiveness with CFF strips. *Engineering Structures* 2003;25:507-16.
- [7] Colotti V, Swamy RN. Unified analytical approach for determining shear capacity of RC beams strengthened with FRP. *Engineering Structures* 2011;33:827-42.
- [8] Dong JF, Wang QY, Guan ZW. Structural behaviour of RC beams externally strengthened with FRP sheets under fatigue and monotonic loading. *Engineering Structures* 2012;41:24-33.

- [9] Lee S, Lee C. Prediction of shear strength of FRP-reinforced concrete flexural members without stirrups using artificial neural networks. *Engineering structures* 2014;61:99-112.
- [10] Shahnewaz M, Machial R, Alam MS, Rteil A. Optimized shear design equation for slender concrete beams reinforced with FRP bars and stirrups using Genetic Algorithm and reliability analysis. *Engineering Structures* 2016;107:151-165.
- [11] Guadagnini M, Pilakoutas K, Waldron P. Shear resistance of FRP RC beams: Experimental study. *Journal of Composites for Construction* 2006;10:464-73.
- [12] Guadagnini M, Pilakoutas K, Waldron P. Shear performance of FRP reinforced concrete beams. *Journal of reinforced plastic composites* 2003;22:1389-470.
- [13] Ahmed EA, El-Salakawy EF, Benmokrane B. Performance evaluation of Glass Fiber Reinforced Polymer shear reinforcement for concrete beams. *ACI Structural Journal* 2010;107:53-62.
- [14] Benmokrane B, Chaallal O, Masmoudi R. Flexural response of concrete beams reinforced with FRP reinforcing bars. *ACI Structural Journal* 1996;91:46-55
- [15] Yost JR, Gross SP, Dinehart DW. Effective moment of inertia for glass fiber-reinforced polymer reinforced concrete beams. *ACI Structural Journal* 2003;100:732-9.
- [16] Toutanji HA, Saafi M. Flexural behaviour of concrete beams reinforced with glass fiber-reinforced polymer (GFRP) bars. *ACI Structural Journal* 2000;97:712-9
- [17] Bischoff PH. Deflection calculation of FRP reinforced concrete beams based on modifications to the existing Branson equation. *Journal of Composites for Construction* 2007;11:5-14.
- [18] Barris C, Torres L, Comas J, Mias C. Cracking and deflections in GFRP RC beams: an experimental study. *Composites Part B: Engineering* 2013;55:580-90.
- [19] Noel M, Soudki K. Estimation of the crack width and deformation of FRP-reinforced concrete flexural members with and without transverse shear reinforcement. *Engineering Structures* 2014;59:393-8.
- [20] Kara IF, Ashour AF, Dundar C. Deflection of concrete structures reinforced with FRP bars. *Composites Part B: Engineering* 2013;44:375-84.
- [21] Rafi MM, Nadjai A. Evaluation of ACI 440 deflection model for fiber-reinforced polymer reinforced concrete beams and suggested modification. *ACI Structural Journal* 2009;106:762-71.
- [22] Ferreira D, Oller E, Barris C, Torres L. Shear strain influence in the service response of FRP reinforced concrete beams. *Composite Structures* 2015;121: 142-153.

- [23] Dundar C, Tanrikulu AK, Frosch RJ. Prediction of load–deflection behavior of multi-span FRP and steel reinforced concrete beams. *Composite Structures* 2015;132: 680-693.
- [24] American Concrete Institute (440.1R-15). Guide for the design and construction of concrete reinforced with FRP bar. Farmington Hills, MI.: 440.1R-15; 2015.
- [25] CEN. Eurocode 2: design of concrete structures. part 1.1: general rules and rules for buildings. Brussels: Comité Européen de Normalisation; 2004.
- [26] Bischoff PH. Re-evaluation of deflection prediction for concrete beams reinforced with steel and FRP bars. *Journal of Structural Engineering, ASCE* 2005;131:363–74.
- [27] Bischoff PH, Gross SP. Equivalent moment of inertia based on integration of curvature. *Journal of Composites for Construction* 2010;15:263-73.
- [28] CEB-FIB. Model Code 1990. Design Code, Comité Euro-International du Béton. Thomas Telford Services Ltd, London 1993.
- [29] CEB-FIB. Model Code 2010. Design Code, Comité Euro-International du Béton. Case Postale 88, CH-1015 Lausanne: Switzerland: the International Federation for Structural Concrete (fib); 2010.
- [30] CurvedNFR. Final report of the CRAFT RTD project CurvedNFR funded by the EU Commission Framework 5 GROWTH programme, contract n° G1ST-CT-2002-50365. <https://cee.sheffield.ac.uk/>; 2015.
- [31] BS EN 12390-3:2009. Testing hardened concrete Part 3: Compressive strength of test specimens. British Standards Institution, London UK 2009.
- [32] BS EN 12390-6:2009. Testing hardened concrete Part 6: Tensile splitting strength of test specimens. British Standards Institution, London UK 2009.
- [33] BS EN 12390-5:2009. Testing hardened concrete Part 5: Flexural strength of test specimens. British Standards Institution, London UK 2009.
- [34] Helal Y, Garcia R, Pilakoutas K, Guadagnini M, Hajirasouliha I. Strengthening of short splices in RC beams using Post-Tensioned Metal Straps. *Materials and Structures* 2016;49:133-47.
- [35] American Concrete Institute (ACI 318-14). Building code requirements for structural concrete (ACI 318-14) and commentary. Farmington Hills, MI.: ACI 318; 2014.
- [36] CEB-158. Analysis of deformations of reinforced concrete structures. *CEB Bulletin d'Information*; 1985.
- [37] Bischoff PH. Effects of shrinkage on tension stiffening and cracking in reinforced concrete. *Canadian Journal of Civil Engineering* 2001;28:363–74.

- [38] Imjai T, Guadagnini M, Pilakoutas K. Estimation of shear crack induced deformations of FRP RC beams. In: Proc in 9th int conf fiber-reinf polymers for rein conc struct. Sydney, Australia, July 13-15, 2009.